Nickel(I) Location and Adsorbate Interactions in Nickel(II)-Exchanged Silicoaluminophosphate Type 5 As Determined by Electron Spin Resonance and Electron Spin Echo Modulation Spectroscopies

Naoto Azuma, Martin Hartmann, and Larry Kevan*

Department of Chemistry, University of Houston, Houston, Texas 77204-5641

Received: November 28, 1994; In Final Form: February 7, 1995[⊗]

The various Ni(I) species formed by thermal reduction and by hydrogen reduction in Ni(II)-exchanged silicoaluminophosphate-5 (NiH−SAPO-5) were studied by electron spin resonance and electron spin echo modulation spectroscopies. Four distinct Ni(I) species are observed in NiH−SAPO-5 heated to 873 K under vacuum: $Ni(I)(O_z)_m(H_2O)_2$ at room temperature where O_z is a zeolitic framework oxygen, $Ni(I)(O_2)_n$ between room temperature and 473 K, $Ni(I)(O_z)_3$ near the center of a 6-ring window (site SII) at temperatures between 473 K and 573 K, and $Ni(I)(O_z)_6$ inside a hexagonal prism (site SI) at temperatures above 773 K. Nickel metal clusters $Ni(O)_n$ are also observed by thermal reduction above 673 K. Two distinct Ni(I) species are observed in NiH−SAPO-5 after hydrogen reduction at 573 K: $Ni(I)(O_z)_6$ at site SI and $Ni(I)(H_2)_n$. A $Ni(I)(O_2)_n$ species is produced in NiH−SAPO-5 after hydrogen reduction, evacuation, and adsorption of water, indicating water decomposition. On adsorption of methanol, Ni(I) in site SI migrates near a 6-ring window and directly coordinates to two methanol molecules and indirectly to one methanol molecule at a greater distance. Ni(I) coordinates to one ethylene by a π-bonding interaction.

Introduction

The aluminophosphate ($AlPO_4$-*n*) and silicoaluminophosphate (SAPO-*n*) molecular sieves belong to a class of microporous materials.[1,2] The SAPO-5 molecular sieve is composed of 4-ring, 6-ring, and 12-ring straight channels, which are interconnected by 6-ring windows (Figure 1). This structure has the $AlPO_4$-5 structure except that the framework phosphorus (P) tetrahedral sites are partially substituted by silicon (Si). This substitution produces a net negative framework charge[3] which after calcination is balanced by H^+ ions which can be partially ion-exchanged by Ni(II) ions. The exchanged product is denoted NiH−SAPO-5. Previously, we have denoted possible cation sites in SAPO-5 by analogy with the designation of cation sites in zeolite X.[4] Site I (SI) is in the center of a hexagonal prism (double 6-ring) that is part of a 6-ring straight channel. Site II (SII) is in the center of a 6-ring window that constitutes part of the side of a 12-ring straight channel. The SII position is in the plane of three oxygens in a 6-ring window. Site II* (SII*) is displaced from site SII toward the 12-ring channel, and site II′ (SII′) corresponds to displacement of site II away from the 12-ring channel toward a double 6-ring.

The catalytic importance of nickel-modified molecular sieves has prompted numerous studies into the physical and chemical nature of the incorporated nickel species. Catalytic activities of such materials depend upon the valence state, location, and dispersion. It has been shown that Ni(I) ions can be active sites in catalytic reactions such as acetylene cyclomerization and ethylene and propylene oligomerization.[5-7] Ni(I) ions formed by reduction of Ni(II) can be stabilized in zeolites and in silica.[8-13] However, the location and the mechanism of Ni(I) formation and stabilization to prevent the formation of $Ni(O)_n$ clusters is not fully understood.

Electron spin echo modulation (ESEM) spectroscopy can supplement electron spin resonance (ESR) spectroscopy to ascertain the environment of an incorporated paramagnetic transition metal ion, and especially its adsorbate coordination.[14]

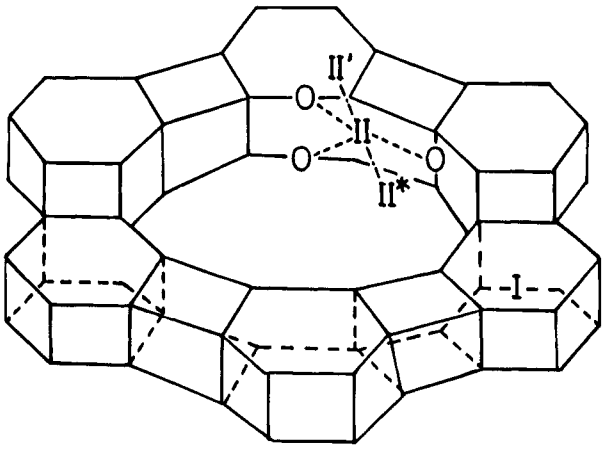

Figure 1. SAPO-5 structure showing possible cation positions. See text for description of the cation positions.

There are few ESR studies on nickel ion introduced into $AlPO_4$-*n* and SAPO-*n* compounds. In this work we have succeeded in producing and stabilizing Ni(I) ions by heating NiH−SAPO-5 under vacuum at temperatures between room temperature and 873 K as well as by hydrogen reduction at 573 K. The location of Ni(I) in NiH−SAPO-5 has been determined by measuring electron spin echo nuclear modulation from framework ^{31}P. The adsorbate geometries of Ni(I) with D_2O, CH_3OD, CD_3OH, and C_2D_4 have been determined by deuterium electron spin echo modulation. The present ESR/ESEM study is the first to investigate the location and assignment of Ni(I) ions in extraframework sites in SAPO-5 molecular sieves for different degrees of dehydration, hydrogen reduction, and adsorbate interaction.

Experimental Section

Samples. H−SAPO-5 was synthesized and calcined according to previous work.[15] NiH−SAPO-5 was prepared by solid-state ion exchange by using $NiCl_2 \cdot 6H_2O$ (Aldrich) and H−SAPO-5, where Ni ions exist in extraframework positions in the

[⊗] Abstract published in *Advance ACS Abstracts,* April 1, 1995.

0022-3654/95/2099-6670$09.00/0

SAPO-5 structure.[16] A mixture of 0.01 g of $NiCl_2 \cdot 6H_2O$ and 1.0 g of H−SAPO-5 was ground well with a mortar and pestle. This solid mixture was pressed in a steel die with 1500 kg cm^{-2} for 20 min to make a disc. Then the disc was heated in a muffle furnace at 873 K in air for 12 h and cooled to room temperature slowly. Before and after the solid-state ion exchange, the color of the sample remained white. Chemical analysis was performed by electron probe microanalysis with a JEOL JXA-8600 spectrometer. The chemical composition of NiH−SAPO-5 was (0.1 atm % Ni, 3.9 atm % Si, 49.8 atm % Al, and 46.2 atm % P). We also prepared liquid-state ion-exchanged samples with calcined H−SAPO-5 and an aqueous solution of $NiCl_2 \cdot 6H_2O$ and $Ni(NO_3)_2$, but we could not obtain any ESR signals in these samples.

Ni−$AlPO_4$-5 was prepared by impregnation by using $NiCl_2 \cdot 6H_2O$ and $AlPO_4$-5[1] according to the following procedure. One gram of calcined $AlPO_4$-5 was added to 20 mL of a 1×10^{-3} M $NiCl_2 \cdot 6H_2O$ solution, and the mixture was stirred at 353 K until the water was completely evaporated. Then, this sample was washed with deionized water at room temperature to remove excess nickel ions on the surface.

Sample Treatment and Measurement. For ESR and ESEM measurements, calcined and hydrated samples were loaded into 3 mm o.d. by 2 mm i.d. Suprasil quartz tubes and pretreated under vacuum ($<10^{-4}$ Torr) at room temperature for 24 h.

To study the change in the coordination environment and assignment of Ni(I) as a function of hydration, the samples were heated under vacuum from 373 to 873 K at intervals of 100 K. For each interval, the temperature was raised slowly and held constant for 24 h. Then ESR spectra were measured at 77 K to detect Ni(I) species produced by this thermal reduction. The sample experiments were also performed on a deuterated sample which was prepared by exposing D_2O to NiH−SAPO-5 after dehydration at 823 K and oxidation with static dry oxygen at 873 K. For ESEM measurements, the samples were heated from room temperature to between 373 and 773 K as noted and held for 24 h. After this thermal treatment, these samples were cooled to 77 K, and helium gas was introduced to a pressure of 30 Torr to increase the thermal conductivity for ESEM measurements near 4 K. Then the samples were sealed. All of the samples for ESEM measurements were stored in liquid nitrogen because the Ni(I) in these samples is reactive toward residual water at room temperature. Hydrogen reduction (100 Torr) was also performed on NiH−SAPO-5 to produce Ni(I) species.

Adsorbate interactions between Ni(I) and water, methanol, and ethylene were also studied. For ESR and ESEM experiments, the samples were prepared as follows: (a) Samples were dehydrated at 823 K ($<10^{-4}$ Torr), the temperature being raised slowly and then held at 823 K for 12 h (dehydration) in order to make totally dehydrated samples. (b) Dry oxygen (500 Torr) was added at room temperature, and the samples were heated at 873 K for 5 h to reoxidize any reduced nickel ions to Ni(II), followed by evacuation at 773 K for 30 min to remove oxygen (activation). (c) In order to prepare Ni(I) species, the samples were reduced by static dry hydrogen (100 Torr) at 573 K for only 30 min to avoid formation of nickel clusters. Then, the reduced samples were evacuated at 573 K for 10 min to remove hydrogen. After this reduction treatment, the color of NiH−SAPO-5 remained white. (d) In order to prepare Ni(I) complexes with various adsorbates, the reduced NiH−SAPO-5 samples were exposed to the room temperature vapor pressure of D_2O (Aldrich), CH_3OD, and CD_3OH (Stohler Isotope Chemicals) and to 100 Torr C_2D_4 (Cambridge Isotope Laboratories). These samples with adsorbates were frozen in liquid nitrogen and sealed. The color of the samples was not changed. During these sample treatments, it is important not to contaminate the samples with trace amounts of water because Ni(I) in SAPO-5 is very reactive toward water.

ESR spectra were recorded with a Bruker ESP-300 X-band spectrometer at 77 K. The magnetic field was calibrated with a Varian E-500 gaussmeter. The microwave frequency was measured by a Hewlett-Packard HP 5342A frequency counter. ESEM spectra were measured near 4 K with a Bruker ESP 380 pulsed ESR spectrometer. Three-pulse echoes were measured by using a $\pi/2-\tau-\pi/2-T-\pi/2$ pulse sequence as a function of time T to obtain the time domain spectrum. To minimize ^{27}Al modulation from zeolitic aluminum in measurements of phosphorus modulation, the τ value was fixed at 0.28 μs.[17] The phosphorus and deuterium modulations were analyzed by a spherical approximation for powder samples in terms of N nuclei at distance R with an isotropic hyperfine coupling A_{iso}.[18] The best fit simulation of an ESEM signal is found by varying the parameters until the sum of the squared residuals is minimized.

Results and Discussion

Thermal Reduction and Location of Nickel Ions in NiH−SAPO-5. NiH−SAPO-5 has a white color after the solid-state ion exchange and does not show any ESR signal at 77 K. Figure 2 shows the changes in the ESR spectra at 77 K for dehydration of NiH−SAPO-5 at several temperatures under vacuum for 24 h. Ni(I) ESR are observed at $g = 2.542$, $g = 2.104$, $g = 2.076$, $g = 2.062$, and $g = 2.044$ after dehydration at room temperature (Figure 2a). Dehydration at 373 K decreased the intensities of the signals at $g = 2.542$ and $g = 2.076$ (Figure 2b). We, therefore, assign the signals $g_{\|} = 2.542$ and $g_{\perp} = 2.076$ to species A and signals $g_1 = 2.104$, $g_2 = 2.062$, and $g_3 = 2.044$ to species B. These species are probably formed by reduction of Ni(II) to Ni(I) by water desorption during the dehydration process. Species A has axially symmetric g anisotropy and is not observed at 473 K (Figure 2c). Species A is stable at room temperature but disappears at 373 K. A species with similar g values to species A has been reported in NiCa−X zeolite after adsorption of H_2O on Ni(I) and assigned to $Ni(I)(O_z)_m(H_2O)_n$,[19] where O_z is a zeolitic framework oxygen. Therefore, we assign species A to $Ni(I)(O_z)_m(H_2O)_n$ at this point, where n will be determined below by ESEM data.

Species B has a rhombic **g** tensor and is stable up to 473 K (Figure 2c). The shape of the ESR signal and the g values of species B in NiH−SAPO-5 are close to those of $Ni(I)(O_2)_n$ in NiH−SAPO-11,[20] formed by O_2 adsorption onto Ni(I). Thus, we assign species B to $Ni(I)(O_2)_n$ where the O_2 is suggested to be derived from water decomposition. Further evidence for this is presented below. Dehydration at 473 K produces another Ni(I) species (C), which has $g_{\|} = 2.492$ and $g_{\perp} = 2.110$ (Figure 2c). Prolonged dehydration at 573 K maximized the intensity of species C with concomittant formation of a broad ESR signal D around $g = 1.931$ (Figure 2d). This ESR signal can also be seen in the absence of nickel in H−SAPO-5 (Figure 3c) after dehydration at 673 K in vacuo. So species D is tentatively assigned to some type of framework defect. Species D is thermally stable to about 673 K (Figure 2e,f) and then begins to decrease in intensity accompanied by an increase in species C′. Species C′ is distinguishable from species C by ^{31}P modulation (see below). Similar thermal reduction by water desorption occurs for Pd(II) to Pd(I) in PdCa−X[21] and PdH−SAPO-11[22] and for Mo(VI) to Mo(V) in MoH−SAPO-5,11.[23]

We have also recently studied the thermal reduction of NiH−SAPO-11[24] which has 10-ring channels instead of the 12-ring channels in SAPO-5. In SAPO-11 the behavior is rather

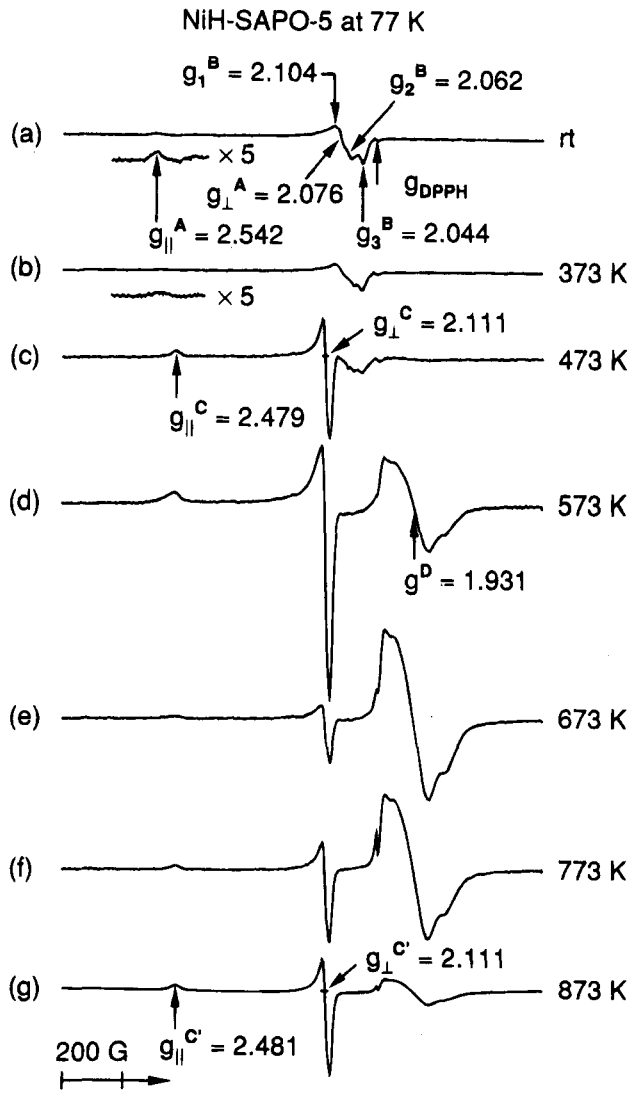

Figure 2. ESR spectra at 77 K of NiH−SAPO-5 (solid-state ion exchange) after dehydration for 24 h at (a) room temperature, (b) 373 K, (c) 473 K, (d) 573 K, (e) 673 K, (f) 773 K, and (g) 873 K.

different. The equivalents of species A and B in SAPO-5 are not observed by similar thermal reduction of NiH−SAPO-11. Instead, only Ni(I) species C is observed above 473 K. Also, no species D is seen by SAPO-11 with smaller channels than in SAPO-5.

After dehydration under vacuum directly at 573 K, mainly species D is produced in NiH−SAPO-5 (Figure 3a). Prolonged dehydration at 673 K decreased the amount of species D and produced a broader, somewhat asymmetric signal around g = 2.21 (species E) characteristic of ferromagnetic or superparamagnetic $Ni(O)_n$ particles[25,26] (Figure 3b) located either in the framework or on the outer surface. Species E was not studied further.

After impregnation of $NiCl_2{\cdot}6H_2O$ into $AlPO_4$-5 to form Ni−$AlPO_4$-5, no ESR signal is observed. Dehydration under vacuum at temperatures below 573 K does not show any ESR signal. Dehydration at 573 K for 24 h begins to form a broad ESR signal around g = 1.931 which is species D. The intensity of species D increases with continued dehydration at higher temperature.

ESEM measurements for Ni(I) species produced by thermal reduction at various temperatures were performed to identify the above Ni(I) species in both NiH−SAPO-5 and deuterated NiD−SAPO-5, which was prepared by D_2O adsorption on a totally dehydrated sample at 823 K. Figure 4 shows three-pulse

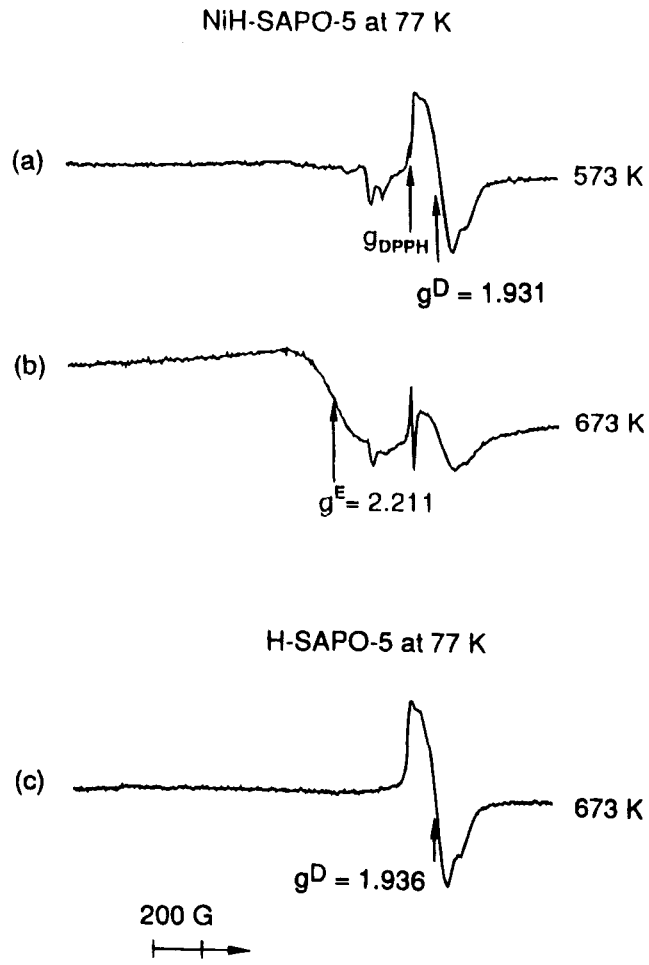

Figure 3. ESR spectra at 77 K of NiH−SAPO-5 after dehydration for 24 h directly at (a) 573 K and (b) 673 K and (c) for H−SAPO-5 after dehydration for 24 h at 673 K.

deuterium ESEM signals of Ni(I) in NiD−SAPO-5 dehydrated under vacuum at room temperature. In this measurement we tried to obtain deuterium modulation signals at two different g values. The data for g = 2.08 corresponds to species A in Figure 2a and shows deuterium modulation (Figure 4a). Ni(I) species A interacts with four deuteriums at 0.29 nm with an isotropic hyperfine coupling of 0.30 MHz. These parameters indicate coordination by two waters ad lead to an assignment of species A as $Ni(I)(O_z)_m(H_2O)_2$.

The ESE signal near g = 2.04 which corresponds to species B shows no deuterium modulation (Figure 4b). This indicates no directly coordinated water around species B and supports the identification of species B as $Ni(I)(O_2)_n$. Deuterium ESEM results for species C in NiD−SAPO-5 after dehydration at both 473 K and 873 K also did not show any deuterium modulation. Therefore, species C only seems to coordinate with zeolitic oxygens.

Table 1 summarizes the ESR parameters for the Ni(I) species produced by thermal reduction of NiH−SAPO-5 at various temperatures. Possible assignments are also given.

ESEM measurements of ^{31}P modulation from Ni(I) species C and C′ produced by thermal reduction at 573 and 773 K were performed and show differences between these two species with very similar ESR parameters. Figure 5 shows the simulated and experimental three-pulse ^{31}P ESEM patterns recorded at τ = 0.27 μs to suppress zeolitic ^{27}Al modulation. There is a significant difference in the ^{31}P modulation patterns between NiH−SAPO-5 dehydrated at 573 and 773 K, indicating that the Ni(I) location in NiH−SAPO-5 changes significantly during

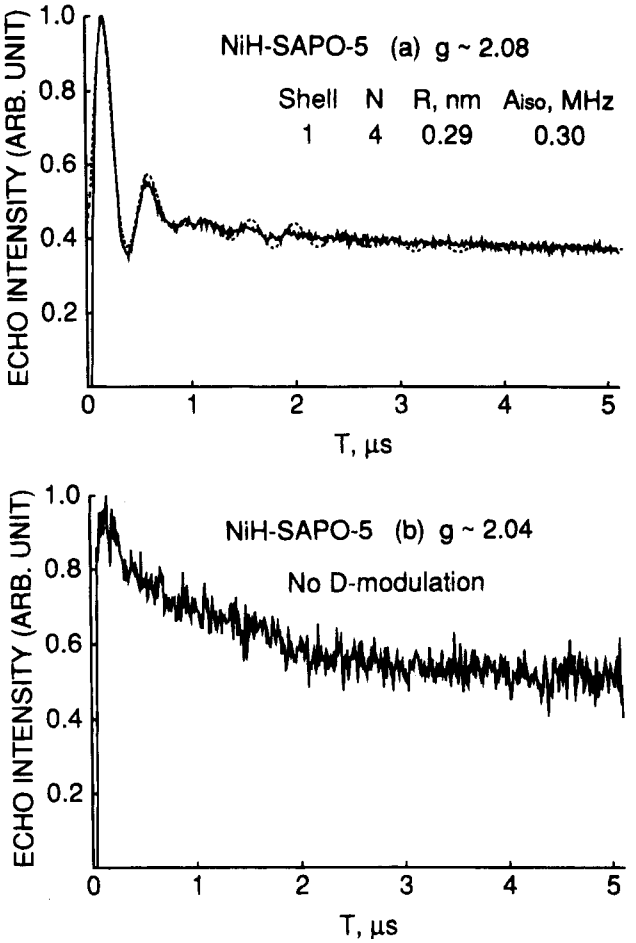

Figure 4. Experimental (—) and simulated (- - -) three-pulse ESEM spectra showing D modulation for NiD−SAPO-5 dehydrated for 24 h at room temperature. Spectra recorded at 4 K at (a) $g = 2.08$ for species A and (b) $g = 2.04$ for species B with $\tau = 0.27$ μs to suppress ^{27}Al modulation.

TABLE 1: ESR g Values at 77 K of Ni(I) in NiH−SAPO-5

reduction method	$g_{\|}$[a]	$g_{\perp}$[a]	species	code
dehydrated at <373 K	2.542	2.076	$Ni(I)(O_z)_m(H_2O)_2$	A
dehydrated at <473 K	2.104	2.062, 2.044	$Ni(I)(O_2)_n$	B
dehydrated at 473−673 K	2.479	2.111	$Ni(I)(Oz)_3$	C
dehydrated above 773 K	2.481	2.111	$Ni(I)(O_z)_6$	C′
dehydrated at <573 K	1.931		framework defect	D
prolonged heating at 673 K	2.21		$Ni(O)_n$	E
reduced in H_2 at 573 K	2.335	2.071	$Ni(I)(H_2)_n$	F
	2.481	2.111	$Ni(I)(O_z)_6$	C′

[a] Estimated uncertainty is ±0.004.

the dehydration process. The simulation parameters for the ^{31}P modulation are listed in Table 2. It is deduced that Ni(I) produced by dehydration at 773 K is located in the center of hexagonal prism sites (SI sites) since the number of nearest phosphorus atoms (N) is 5.2, while Ni(I) ions at 573 K are located near SII sites, since $N = 3.5$. According to previous work on Ni−faujasite,[27] NiNa−X,[19] and NiNa−Y,[28] the Ni(II) ions at SI sites are more stable than those in SI′, SII, and SII′ sites in zeolites when they are dehydrated above 723 K. Thus, our conclusions about the Ni(I) locations of species C and C′ seem consistent with previous work.

Hydrogen Reduction and Location of Nickel(I) in NiH−SAPO-5. When NiH−SAPO-5 is heated in hydrogen, weak ESR signals begin to appear around 473 K. The ESR signal intensities are increased by raising the reduction temperature. Figure 6a shows the ESR spectrum of NiH−SAPO-5 after hydrogen reduction at 573 K for 30 min in which the sample

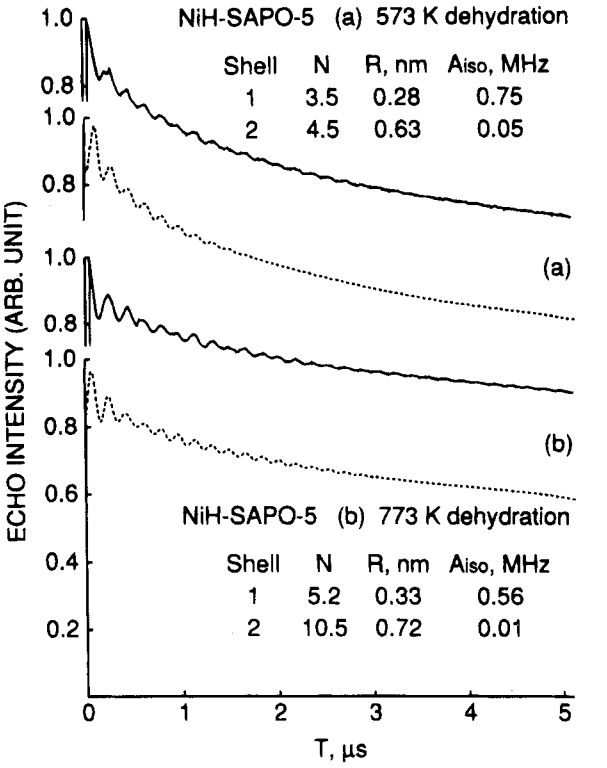

Figure 5. Experimental (—) and simulated (- - -) three-pulse ESEM spectra showing ^{31}P modulation for NiH−SAPO-5 (a) dehydrated for 24 h at 573 K and observed at $g_{\perp} = 2.1$ for species C and (b) dehydrated for 24 h at 773 K and observed at $g = 2.1$ for species C′. Spectra recorded at 4 K at with $\tau = 0.27$ μs to suppress ^{27}Al modulation.

TABLE 2: Simulation Parameters of Three-Pulse ^{31}P ESEM for Ni(I) in NiH−SAPO-5

dehydration	shell	N[a]	R,[b] nm	A_{iso},[c] MHz	site
573 K	1	3.5	0.28	0.92	SII
	2	4.5	0.60	0.10	
773 K	1	5.2	0.33	0.56	SI
	2	10.5	0.72	0.01	

[a] Number of phosphorus atoms. [b] Distance between Ni(I) and phosphorus; estimated uncertainty is ±0.01 nm. [c] Isotropic hyperfine coupling constant; estimated uncertainty is ±10%. Spectra were recorded at $g = 2.11$.

still contained hydrogen gas. Two Ni(I) ESR signals are observed. Species C′ is the same as observed by thermal reduction (see Figure 2). Species C′ remains after evacuation of the hydrogen gas at room temperature (Figure 6b). Species F disappears after evacuation of the hydrogen at room temperature (Figure 6b), but it is readily regenerated by subsequent exposure to hydrogen. Thus, species F is assigned to Ni(I)-$(H_2)_n$. Species C′ appears to show a small increase on evacuation of the hydrogen.

The three-pulse ^{31}P ESEM patterns for species C′ formed by hydrogen reduction are the same as for species C′ formed by thermal reduction. Therefore, we conclude that species C′ formed by both reduction procedures is located in the same SI site in SAPO-5. We also tried to obtain ^{31}P ESEM data for species F, but the result was too noisy to analyze.

Adsorbate Interactions of Ni(I) in NiH−SAPO-5. In order to study adsorbate interactions with Ni(I) in the SI site in NiH−SAPO-5, we reduced NiH−SAPO-5 with hydrogen. Before an adsorbate is added, the hydrogen-reduced samples are evacuated at 573 K for 10 min so only Ni(I) in site SI remains (Figure 6b). The adsorbate is then exposed to the sample for about 5 min at room temperature, and the sample is quenched to 77 K.

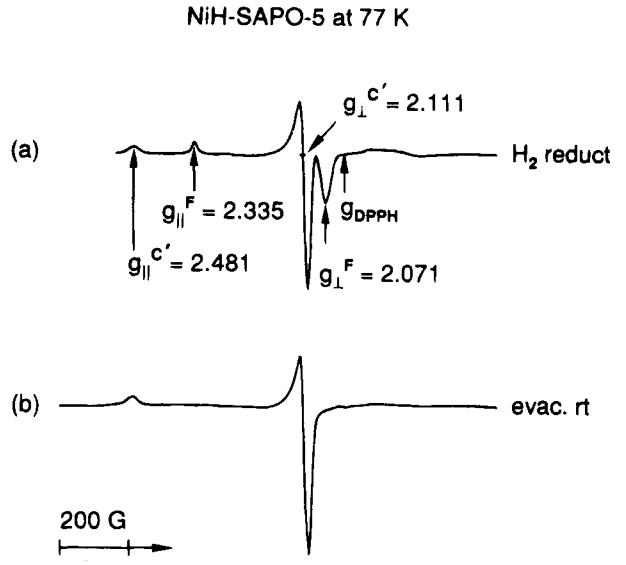

Figure 6. ESR spectra at 77 K of NiH−SAPO-5 (a) after reduction with H_2 for 30 min at 573 K and (b) after 10 min evacuation of (a) at room temperature.

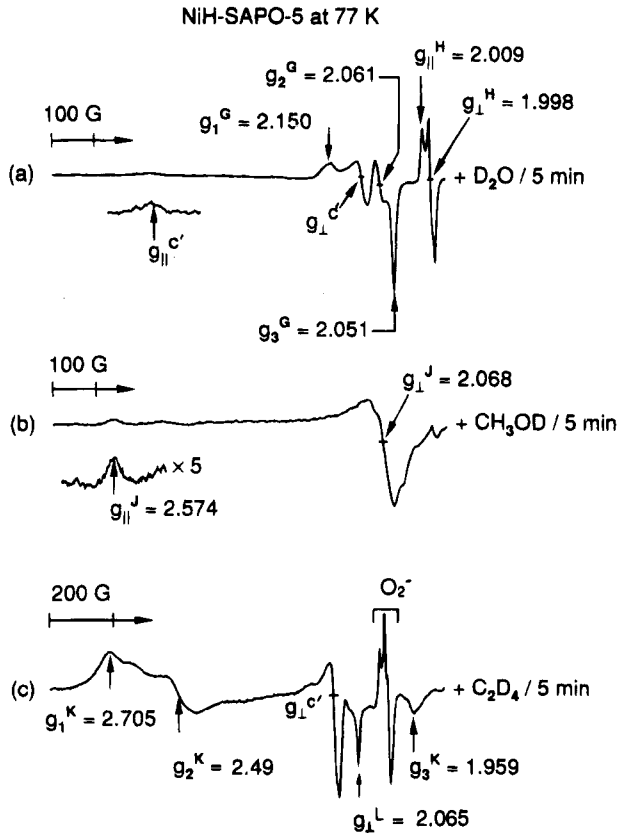

Figure 7. ESR spectra at 77 K of NiH−SAPO-5 after H_2 reduction and evacuation and after subsequent adsorption of (a) D_2O, (b) CH_3OD, and (c) C_2D_4 for 5 min at room temperature.

The adsorption of D_2O (vapor pressure ~23 Torr) at room temperature on NiH−SAPO-5 leads to the formation of species G with a rhombic **g** tensor (Figure 7a). Adsorption of O_2 instead of D_2O also leads to species G, so it is assigned to $Ni(I)(O_2)_n$. Somewhat similar g values (g_1 = 2.16, g_2 = 2.09, and g_3 = 2.055) have been assigned to $Ni(I)(O_2)_n$ in NiCa−Y zeolite.[9] ESE for species G observed at g_1 = 2.150 and g_3 = 2.051 showed no deuterium modulation, consistent with this chemical assignment for species G. We note that species B and G are the same chemically, although their g_1 values are somewhat different. After D_2O adsorption, species C′ only retains 10% of its intensity in NiH−SAPO-5, so most of it reacts with D_2O to form species G and an additional species H with $g_\parallel$ = 2.009 and $g_\perp$ = 1.998 and a characteristic shape which can be assigned to an O_2^- radical.[9]

TABLE 3: ESR g Values of Ni(I) in Various Matrices

matrix	adsorbate	species	$g_\parallel$	$g_\perp$	ref
NiH−SAPO-5	D_2O^b	$Ni(I)(O_2)_n$	2.150	2.061,2.051	this work[a]
NiH−SAPO-11	D_2O^b	$Ni(I)(O_2)_n$	2.135	2.062,2.048	20
NiCa−X	H_2O	$Ni(I)(H_2O)_3$	2.471	2.061	19
NiH−SAPO-5	CH_3OD^b	$Ni(I)(CH_3OD)_2$	2.574	2.063	this work[a]
NiH−SAPO-11	CH_3OD^b	$Ni(I)(CH_3OD)_1$	2.463	2.084	20
NiCa−X	CH_3OH	$Ni(I)(CH_3OH)_3$	2.461	2.084	19
NiH−SAPO-5	$C_2D_4^b$	$Ni(I)(C_2D_4)_1$	2.705	2.489,1.959	this work[a]
NiH−SAPO-11	C_2D_4	$Ni(I)(C_2D_4)_1$	2.693	2.463,1.970	30
NiCa−X	C_2H_4	$Ni(I)(C_2D_4)$	2.643	2.46,1.973	19
NiLa−Y	C_2H_4	$Ni(I)(C_2D_4)$	2.71	2.57,1.96	25

[a] Estimated uncertainty in g is ±0.004. [b] The adsorbate was added for 5 min at room temperature after evacuation for 10 min at 573 K followed by hydrogen reduction at 573 K.

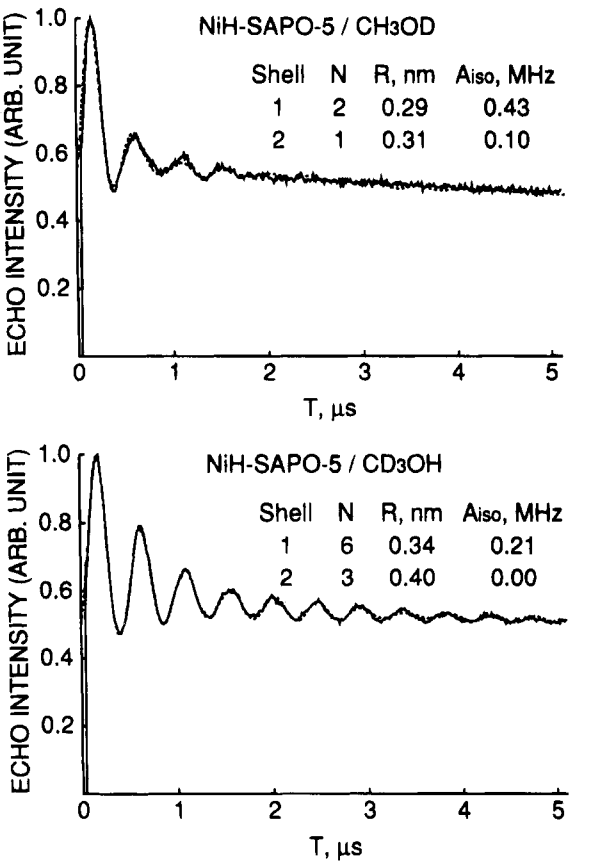

Figure 8. Experimental (—) and simulated (- - -) three-pulse ESEM spectra recorded at 4 K of NiH−SAPO-5 after H_2 reduction, evacuation, and (a) CH_3OD and (b) CD_3OH absorption. Spectra recorded at $g \approx 2.06$ for species J with τ = 0.27 μs to suppress ^{27}Al modulation.

The ESR spectrum recorded after CH_3OD adsorption at room temperature on NiH−SAPO-5 is shown in Figure 7b. Species J is assigned as axially symmetric with $g_\parallel$ = 2.574 and $g_\perp$ = 2.068, but the $g_\perp$ region seems to show some deviation from this. Since the g values differ from those of Ni(I) species C′, methanol coordination is indicated as shown below from ESEM data. In contrast, Ni(I) in NiCa-X zeolite decomposes adsorbate methanol.[19]

Figure 7c shows the ESR spectrum at 77 K after the adsorption of C_2D_4 (pressure 100 Torr) at room temperature on NiH−SAPO-5 containing Ni(I). Ni(I) species C′ is still quite prominent as seen by its $g_\perp$ feature so only a fraction of Ni(I)

TABLE 4: Simulation Parameters of Three-Pulse ^2H ESEM of Ni(I) in NiH−SAPO-5 Treated with Various Adsorbates

adsorbate	shell	N^a	R,[b] nm	A_{iso},[c] MHz	molecules
D_2O			[d]		
CH_3OD[e]	1	2	0.29	0.43	2
	2	1	0.31	0.10	1
CD_3OH[e]	1	6	0.34	0.21	2
	2	3	0.40	0.0	1
C_2D_4[f]	1	4	0.35	0.22	1

[a] Number of deuterium atoms. [b] Distance between Ni(I) and deuterium; estimated uncertainty is ±0.01 nm. [c] Isotropic hyperfine coupling constant; estimated uncertainty is ±10%. [d] Electron spin echo signal with no deuterium modulation was observed. [e] ESEM was recorded at $g = 2.07$ for species J. [f] ESEM was recorded at $g = 1.96$ for species K.

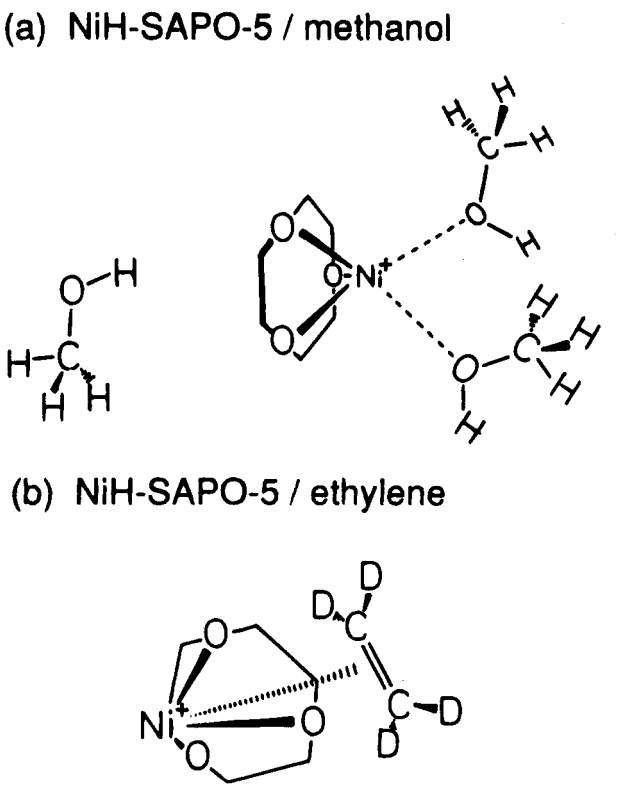

Figure 9. (a) Schematic diagram of Ni(I) a site II* in NiH−SAPO-5 directly coordinated to two methanol molecules in the same 12-ring channel and indirectly coordinated to one methanol molecule in an adjacent 12-ring channel. (b) Schematic representation of Ni(I) coordinated to ethylene in NiH−SAPO-5 showing one weakly coordinated ethylene molecule in a 12-ring channel.

migrates from site I to interact with ethylene. A new species (K) is observed and can be assigned to a $Ni(I)C_2D_4$ complex. This is confirmed by the ESEM data reported below. Similar ethylene complexes to species K are found in NiCa−X[19] and NiLa−Y,[29] and in NiH−SAPO-11.[30] In NiH−SAPO-11, with a smaller channel (10-ring) than in NiH−SAPO-5 (12-ring), Ni(I) needs temperatures of about 323 K to migrate in order to coordinate with ethylene. Another observed species (L) is perhaps due to Ni^+ coordination with traces of water introduced during exposure to ethylene. Species L seems to be the same as species G formed during D_2O adsorption.

Table 3 summarizes the ESR parameters of Ni(I) in NiH−SAPO-5 with various adsorbates and of the related microporous materials NiH−SAPO-11, NiCa−X, and NiLa−Y. Species assignments are also given.

The experimental and simulated three-pulse ESEM spectra for NiH−SAPO-5 with adsorbed methanol (CH_3OD and CD_3OH) are shown in Figure 8. Simulations required a two-shell model (Table 4). For adsorbed CH_3OD, Ni(I) interacts with two deuteriums, i.e., two molecules of methanol, at 0.29 nm, which is a direct coordination distance, and with one more deuterium, i.e., one molecule of methanol, at 0.31 nm, which is an indirect coordination distance. The ESEM simulation parameters for CD_3OH are consistent with this. The indirectly coordinated methanol must be oriented in such a way that its methyl group is directed toward the Ni(I) ion to give a Ni(I)−D distance of 0.43 nm for CH_3OD and 0.31 nm for CD_3OH. This more distant methanol molecule is likely in an adjacent 12-ring channel. As discussed above, the Ni(I) ions are located in site SI before methanol adsorption. So methanol coordination implies migration of Ni(I) from site I to a more accessible site like site II or II*. Figure 9 shows this methanol coordination geometry for Ni(I). This geometry, with Ni(I) at site II* with three framework oxygens and two methanol molecules directly coordinated, should exhibit deviations from axial g anisotropy as seem to be observed. Similar methanol coordination has been reported for Cu(II) in Cu(II)-exchanged zeolite rho[31] and in CuH−SAPO-5.[15]

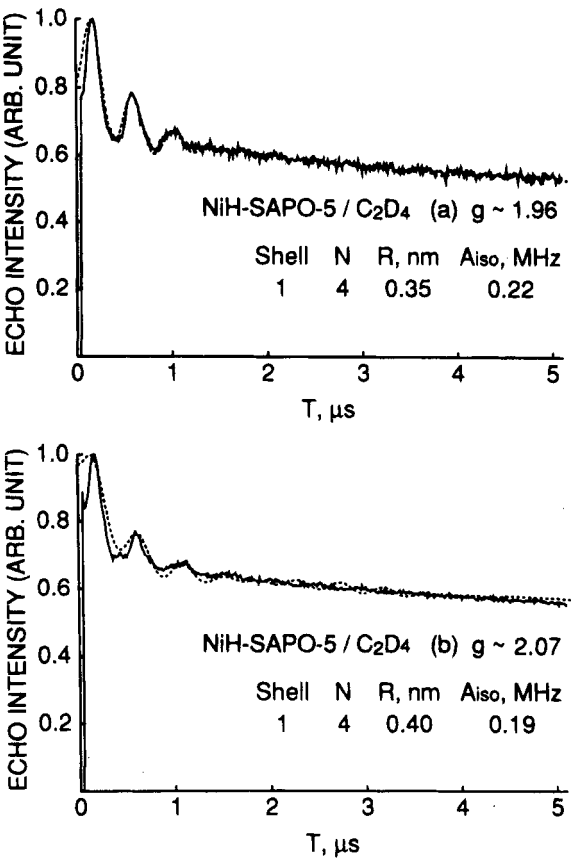

Figure 10. Experimental (—) and simulated (- - -) three-pulse ESEM spectra at 4 K of NiH−SAPO-5 after H_2 reduction, evacuation, and C_2D_4 adsorption. Spectra recorded at $g = 1.96$ for species K.

The experimental and simulated three-pulse ESEM spectra for NiH−SAPO-5 with adsorbed C_2D_4 were performed at $g = 1.96$ (Figure 10). Species K shows interaction with four equivalent deuteriums at a distance of 0.35 nm (Table 4). This suggests that one ethylene is coordinated with its molecular plane perpendicular to a line toward Ni(I), consistent with π-bonding. Figure 9 shows this ethylene-coordinated geometry to Ni(I). Similar coordination of Ni(I)-ethylene was suggested in NiCa−X,[19] where Ni(I) is located in site SII, but no coordination of Ni(I) to ethylene was found for Ni(I) located in site SI in zeolite X[19] or in NiH−SAPO-11.[20]

Conclusions

ESR and ESEM results have revealed thermal and hydrogen reduction of Ni(II) to Ni(I) and the probable locations of Ni(I) and its adsorbate interactions in NiH−SAPO-5. Thermal reduction of NiH−SAPO-5 produces $Ni(I)(O_z)_m(H_2O)_2$, which is only stable slightly above room temperature, $Ni(I)(O_2)_n$, which is stable to 473 K, Ni(I) near site SII, which is produced above 473 K to about 673 K, and Ni(I) in site SI above 773 K. Above 573 K, $Ni(0)_n$ clusters inside SAPO-5 are also formed. Hydrogen reduction at 573 K generates two Ni(I) species, Ni(I) in site SI and $Ni(I)(H_2)_n$. The $Ni(I)(H_2)_n$ complex is stable only in the presence of hydrogen. $Ni(I)(O_2)_n$ is produced in NiH−SAPO-5 after adsorption of water, indicating water decomposition. The Ni(I) complex generated in NiH−SAPO-5 after methanol adsorption has two directly coordinated methanols and another indirectly coordinated methanol in an adjacent 12-ring channel. The adsorption of C_2D_4 on Ni(I) in NiH−SAPO-5 produces a $Ni(I)(C_2D_4)$ species corresponding to a coordination distance of 0.35 nm.

Acknowledgment. This research was supported by the National Science Foundation and the Robert A. Welch Foundation. We thank J. Michalik for help with sample preparations and useful discussions.

References and Notes

(1) Wilson, S. T.; Lok, B. M.; Flanigen, E. M. U.S. Patent 4,310,440, 1982.

(2) Wilson, S. T.; Lok, B. M.; Messina, C. A.; Cannan, T. R.; Flanigen, E. M. *J. Am. Chem. Soc.* **1982**, *104*, 1146.

(3) Flanigen, E. M.; Lok, B. M.; Patton, R. L.; Wilson, S. T. In *New Developments in Zeolite Science and Technology*; Proceedings of the 7th International Zeolite Conference; Murakami, Y., Iijima, A., Ward, J. W., Eds.; Elsevier: Amsterdam, 1986; pp 103−112.

(4) Kevan, L. *Rev. Chem. Intermed.* **1987**, *8*, 53.

(5) Kazansky, V. B.; Elev, I. V.; Shelimov, B. N. *J. Mol. Catal.* **1983**, *21*, 265.

(6) Bonneviot, L.; Olivier, D.; Che, M. *J. Mol. Catal.* **1983**, *21*, 415.

(7) Moller, B. W.; Kemball, C.; Leach, H. F. *J. Chem. Soc., Faraday Trans. 1* **1983**, *79*, 453.

(8) Rabo, J. A.; Angell, C. L.; Kasai, P. H.; Shomaker, V. *Discuss. Faraday Soc.* **1966**, *41*, 328.

(9) Garbowski, E. D.; Vedrine, J. C. *Chem. Phys. Lett.* **1977**, *48*, 550.

(10) Olivier, D.; Richard, M.; Che, M.; Bozon-Verduraz, F.; Clarkson, R. B. *J. Phys. Chem.* **1980**, *84*, 420.

(11) Olivier, D.; Richard, M.; Che, M. *Chem. Phys. Lett.* **1978**, *60*, 77.

(12) Elev, I. V.; Pershin, A. N.; Shelimov, B. N.; Kazansky, V. B. *Kinet. Katal.* **1982**, *23*, 936.

(13) Garbowski, E. D.; Mathieu, M. V.; Primet, M. *Chem. Phys. Lett.* **1977**, *49*, 247.

(14) Kevan, L. *Acc. Chem. Res.* **1987**, *20*, 1.

(15) Chen, X.; Kevan, L. *J. Am. Chem. Soc.* **1991**, *113*, 2861.

(16) Beyer, H. K.; Karge, H. G.; Borbely, G. *Zeolites* **1988**, *8*, 79.

(17) Fenter, P.; Eisenberger, P.; Li, J.; Camillone, N., III; Bernasek, S.; Scoles, G.; Ramanarayanan, T. A.; Liang, K. S. *Langmuir* **1991**, *95*, 4777.

(18) Kevan, L. In *Time Domain Electron Spin Resonance*; Kevan, L., Schwartz, R. N., Eds.; Wiley: New York, 1979; Chapter 8.

(19) Michalik, J.; Narayana, M.; Kevan, L. *J. Phys. Chem.* **1984**, *88*, 5236.

(20) Azuma, N.; Lee, C. W.; Kevan, L. *J. Phys. Chem.* **1994**, *98*, 1217.

(21) Michalik, J.; Narayana, M.; Kevan, L. *J. Phys. Chem.* **1985**, *89*, 4553.

(22) Lee, C. W.; Yu, J. S.; Kevan, L. *J. Phys. Chem.* **1992**, *96*, 7747.

(23) Lee, C. W.; St. Pierre, T.; Azuma, N.; Kevan, L. *J. Phys. Chem.* **1993**, *97*, 11811.

(24) Azuma, N.; Kevan, L. *J. Phys. Chem.* **1995**, *99*, 5083.

(25) Che, M.; Richard, M.; Olivier, D. *J. Chem. Soc., Faraday Trans. 1* **1980**, *76*, 1526.

(26) Bonneviot, L.; Che, M.; Olivier, D.; Martin, G. A.; Freund, E. *J. Phys. Chem.* **1986**, *90*, 2112.

(27) Olson, D. H. *J. Phys. Chem.* **1968**, *72*, 4366. Dempsey, E.; Olson, D. H. *J. Phys. Chem.* **1970**, *74*, 305.

(28) Gallezot, P.; Imelik, B. *J. Phys. Chem.* **1973**, *77*, 652.

(29) Schoonheydt, R. A.; Vaesen, I.; Leeman, H. *J. Phys. Chem.* **1989**, *93*, 1515.

(30) Hartmann, M.; Kevan, L. Unpublished work.

(31) Anderson, M. W.; Kevan, L. *J. Phys. Chem.* **1986**, *90*, 6452.

JP9431494